1-1-2015

Study on surface asperity flattening in cold quasi-static uniaxial planar compression by crystal plasticity finite element method

Hejie Li
University of Wollongong, hejie@uow.edu.au

Zhengyi Jiang
University of Wollongong, jiang@uow.edu.au

Dongbin Wei
University of Wollongong, dwei@uow.edu.au

Jianzhong Xu
Northeastern University

Xiaoming Zhang
Northeastern University

See next page for additional authors

Study on surface asperity flattening in cold quasi-static uniaxial planar compression by crystal plasticity finite element method

Abstract

In order to study the surface asperity flattening in a quasi-static cold uniaxial planar compression, the experimental results of atomic force microscope and electron backscattered diffraction have been employed in a ratedependent crystal plasticity model to analyze this process. The simulation results show a good agreement with the experimental results: in this quasi-static deformation process, lubrication can hinder the surface asperity flattening process even under very low deformation rate. However, due to the limitation of the model and some parameters, the simulation results cannot predict all the properties in detail such as S orientation {123}and the maximum stress in sample compressed without lubrication. In addition, the experimental results show, with an increase in gauged reduction, the development of Taylor factor, and CSL boundaries show certain tendencies. Under the same gauged reduction, friction can increase the Taylor factor and $\Sigma = 7$.

Keywords

surface, study, cold, quasi, static, uniaxial, planar, asperity, compression, method, crystal, plasticity, finite, element, flattening

Disciplines

Engineering | Science and Technology Studies

Publication Details

Li, H., Jiang, Z., Wei, D., Xu, J., Zhang, X., Gong, D. & Han, J. (2015). Study on surface asperity flattening in cold quasi-static uniaxial planar compression by crystal plasticity finite element method. Tribology Letters, 58 (3), 1-10.

Authors

Hejie Li, Zhengyi Jiang, Dongbin Wei, Jianzhong Xu, Xiaoming Zhang, Dianyao Gong, and Jingtao Han

Study on surface asperity flattening in cold quasi-static uniaxial planar compression by Crystal Plasticity Finite Element Model

Hejie Li[1*], Zhengyi Jiang[1,*], Dongbin Wei[1, 2], Jianzhong Xu[3], Xiaoming Zhang[3], Dianyao Gong[3], Jiangtao Han[4]

[1] School of Mechanical, Materials and Mechatronic Engineering, University of Wollongong, NSW2522, Australia

[2]School of Electrical, Mechanical and Mechatronic Systems, Faculty of Engineering and Information Technology, University of Technology, Sydney, NSW 2007, Australia

[3]State Key Laboratory of Rolling and Automation, Northeastern University, Shenyang, Liaoning 110004, China

[4]School of Materials Sciences and Engineering, University of Sciences and Technology Beijing, Beijing 100083, PR China

Email: hl993@uowmail.edu.au, jiang@uow.edu.au

Abstract: In order to study the surface asperity flattening in a quasi-static cold uniaxial planar compression, the experimental results of Atomic Force Microscope (AFM) and Electron Backscattered Diffraction (EBSD) have been employed in a rate-dependent crystal plasticity model to analyse this process. The simulation results show a good agreement with the experimental results: in this quasi-static deformation process, lubrication can hinder the surface asperity flattening process even under very low deformation rate. However, due to the limitation of the model and some parameters, the simulation results cannot predict all the properties in details such as S orientation {123} <634>, and the maximum stress in sample compressed without lubrication. In addition, the experimental results show, with an increase of gauged reduction, development of Taylor factor and CSL boundaries show the certain tendencies. Under the same gauged reduction, friction can increase the Taylor factor and Σ=7.

Keywords: Quasi-static, Surface asperity, Cold uniaxial planar compression (CUPC), Crystal plasticity finite element modelling, Texture

1 Introduction

In metal forming process, deformation rate is an important parameter, which has a significant influence on surface quality of the final products. Practically, most metal materials are rate

dependent material. Therefore, as an important parameter, strain rate can influence many prosperities of metal forming products, such as strength, stress, facture, microstructure, work hardening, plasticity and so on. There are many literatures mentioned about the strain rate effects. Liu et al. [1] found that with an increase of strain rate, the yield stress of single-crystal copper increases rapidly, the formed shear band width also increases. Travis et al. [2] analysed the relationship between strain, strain rate and temperature in severe plastic deformation of copper, and pointed out the nanoscale-twinning's development at the different strain rates and deformation temperatures. Serebrinsky et al. [3] investigated the effect of strain rate on the stress corrosion crack propagation rate and found out that the accelerating effect of the strain rate was always higher for intergranular stress corrosion cracking than for transgranular stress corrosion cracking. They [4] also pointed that by increasing the strain rate a monotonic increase of the log crack propagation rate takes place. Wu et al [5] analysed the inverse effect of strain rate on mechanical behavior and phase transformation of superaustenitic stainless steel, and pointed out that the ductility of superaustenitic stainless steel increases significantly with an increase in the strain rate. Papakaliatakis [6] analysed the effect of strain rate on crack growth in aluminum alloy 1100-0. He found that compared to the plasticity theory, the strain rate dependent model would predict a lower load for crack initiation. Urcola et al. [7] investigated the effect of changing strain rate on stress-strain behavior during high temperature deformation. They found out that in both the ferritic stainless steel and the Al-l % Mg alloy, the flow stress is dependent only on the instantaneous strain rate, but not on the way this strain rate is reached. Takuda et al [8] investigated the effect of strain rate on deformation behavior of an Mg-8.5Li-1Zn alloy sheet at room temperature. They reported that at room temperature, ductility decreases with the increase in strain rate and the stress is also sensitive to the strain rate. Bhattacharyya et al [9] analysed the effect of strain rate on deformation texture in Oxygen-free high thermal conductivity (OFHC) copper. They found that the increase in strain rate causes increase in strain hardening which thereby influences the texture. Zhang et al [10] studied the effect of strain rate on microstructure of polycrystalline oxygen-free high conductivity copper severely deformed at liquid nitrogen temperature. Kodeeswaran et al [11] analysed the effect of strain rate on nanocrystalline surface formation in controlled ball impact process in AISI 304 SS. They pointed out the surface roughness of the samples treated depends on the strain rate exerted and sample traveling velocity. Eghbali et al [12] analysed the effect of strain rate on the microstructural development of the microalloyed steel by using the torsion equipment. They found that at lower strain rate the continuous dynamic recrystallised grains become larger, under high strain rate deformation the time for grain growth is diminished and

the coalescence of continuous dynamic recrystallised grains is inhibited. Percy [13] analysed the influence of strain rate on the forming limit diagram of sheet metal in tensile test. He pointed out that the strain hardening exponent falls as the strain increases. Based on dislocation theory, Qin et al [14] analysed the mechanism of strain rate effect. They proposed that strain rate criteria rather than stress criteria should be satisfied when a metal is fully yielded at a given strain rate.

However, there are no literatures which mentioned about the strain rate effect on surface asperity flattening (surface roughness) process. On the basis of experimental results, we previously investigated the relationship between the surface asperity, friction [15], and grain size [16] by applying 2D crystal plasticity finite element model. We also analysed the relationship between the surface asperity flattening, reduction and texture and grain orientation by a 3D surface roughness model [17]. The influences of high strain rate on surface asperity flattening and micro-texture evolution were investigated in previous study [15-17]. Therefore in this study, influence of quasi-static deformation (low strain rate, $0.001s^{-1}$) on surface asperity flattening process has been analysed. Both simulation and experimental results show a good agreement: they all show the influence of lubrication on surface asperity flattening includes the development of surface roughness, stress and texture. However, due to the limitation of the model and some parameters, the simulation results cannot predicate all the properties in details. In experiment, with an increase of gauged reduction, development of Taylor factor and coincidence site lattice (CSL) boundary also show a certain tendency. Under the same gauged reduction, friction increases the Taylor factor and the value of Σ7 obviously. On the other hand, lubrication can promote the migration of Σ17.

2 Experimental equipment and procedures

2.1 Sample

In this study, Al6061 has been chosen as the material for test. Originally, all samples received an annealing heat-treatment: all samples were heated to 500°C holding for 2 hours, and then cooled in furnace. The annealed microstructure is shown in Fig. 1. In order to generate the required surface roughness, samples were ground by the sand paper of No P220. Roughness of sample all ranges as: R_a is about 0.72μm, R_q is about 0.84μm, the minimum error is about 0.02μm. The original surface asperity is shown in Fig. 2.

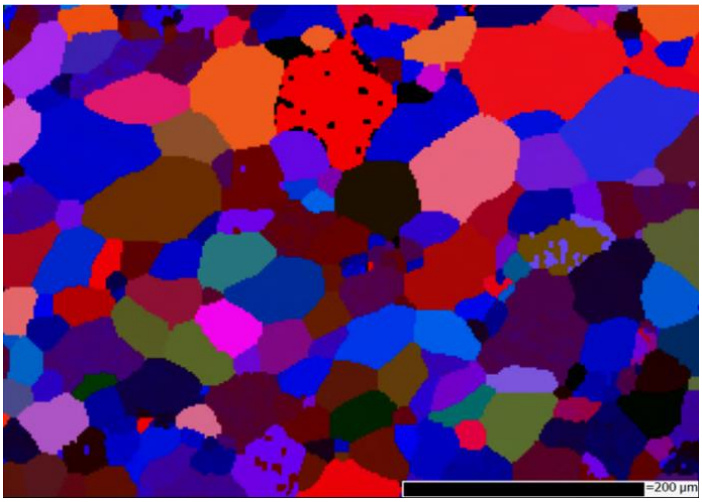

Figure 1 Microstructure after annealing heat-treatment

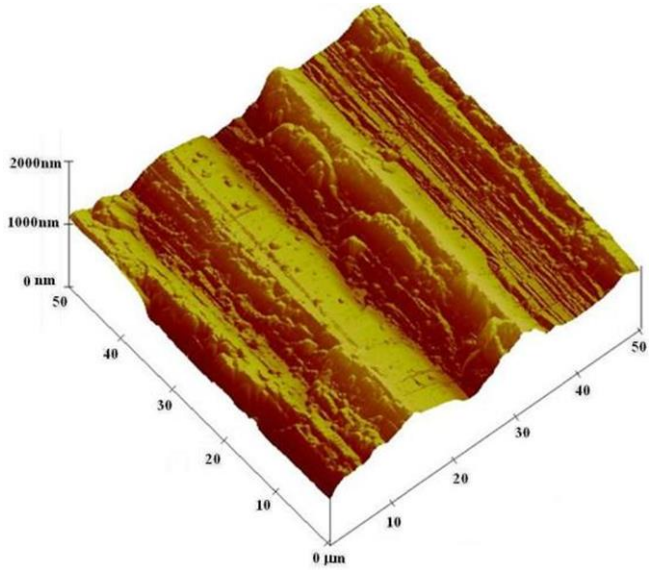

Figure 2 Original surface asperity of sample

Al 6061 T5 is a typical FCC (face centered cubic) metal. Normally in FCC metal, it has 12 {111} <110> slip systems: 4 slip planes and three slip directions in each slip plane. The slip systems are shown in Fig. 3 [29].

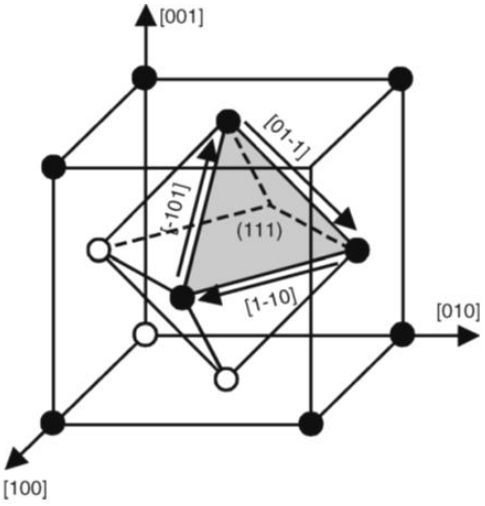

Figure 3 Slip systems in FCC metal Al

2.2 Equipment

After a fully annealed heat treatment, Al6061 samples (10 mm×10 mm×6 mm) were compressed on a channel die, while samples were constrained in the transverse direction. In order to reduce the influence of tool, the compressing tool is polished smoothly (surface roughness is about 10 nm) and flat. The deformation ranges from 0 to 60 %. The compressing channel die includes two parts: compressing mould and tool [17, 18]. For convenience of handling sample, the compressing mould includes two separate parts which are assembled by a screw. The compression test was carried out by the INSTRON servo-hydraulic testing machine. The employed strain rate is about 0.001 s^{-1}. In this study, Molly bond is chose as the lubricant during the compression. Friction coefficient between the tool and sample is about 0.2. Reduction can be defined as:

$$R = \frac{\Delta h}{H_0}\% \tag{1}$$

where, R is the reduction, Δh is the height increment, H_0 is the sample height before compression.

2.3 Cold Uniaxial Planar Compression (CUPC) Process

The compression was carried out in INSTRON servo-hydraulic testing machine. The testing schedule is shown in Table 1. A displacement is the shortest distance from the initial to the final position of a point.

Table 1 Compression schedule

Samples	Height (mm)	Reduction (%)	Strain rate (s^{-1})	Displacement rate (mm/min)	Displacement (mm)	Height after compression (mm)
N1/L1	6.3	0	0.001	0	0	6.3
N2/L2	6.3	20	0.001	-.3.39	1.26	5.04
N3/L3	6.3	40	0.001	-2.96	2.51	3.79
N4/L4	6.3	60	0.001	-2.48	3.78	2.52

On the basis of static deformation, strain rates are chosen as $0.001s^{-1}$. Normally, it is difficult to control the strain rate on the INSTRON servo-hydraulic testing machine, and also in the metal forming process the strain rate does not keep the same value. There are two solutions: firstly in very short deforming process, the variation of strain rate is not significant, and in some cases the strain rate in this kind process can be considered as a constant; the other one is to use other parameters to practise the control. In this case the strain rate is very low and the deformation is a quasi-static process, therefore the strain rate can be considered as a constant. In this study, the displacement rate is used to replace the strain rate [17-21]. The relationship between the strain rate and displacement rate is

$$\varepsilon = \ln\frac{H}{H_0} = \ln\frac{H_0 - \Delta H}{H_0},\ \dot{U} = \Delta H / \Delta t = \Delta H \cdot \dot{\varepsilon} / \varepsilon \tag{2}$$

where H_0, H, ΔH are the original height, the height after compression and the height increment respectively. ε is the true strain. Δt is the time of deformation. $\dot{U}$ is the displacement rate of sample in the compression.

3 Crystal plasticity finite element model

3.1 Assumptions of single grain model

For crystal plasticity, single crystal model is based on five following assumptions: (1) neglect other deformation mechanisms, slip is the only available one; (2) activated slip system is {111}<110>; (3) twinning exists in the system with low stack fault energy metal; (4) in the same metal, all the slip systems have the same critical shearing stress; (5) the trans-granular slip is homogeneous. The velocity gradient for the plastic deformation is shown as [18, 19, 21-24]

$$\dot{F}^{p} \cdot F^{p^{-1}} = \sum_{\alpha=1}^{n} \dot{\gamma}^{\alpha} S_0^{\alpha} = \sum_{\alpha=1}^{n} \dot{\gamma}^{\alpha} u_0^{\alpha} \otimes v_0^{\alpha} \tag{3}$$

where F^{p} denotes the deformation gradient due to the plastic deformation. $\dot{\gamma}^{\alpha}$ is the shearing rate on the slip system α, and u_0^{α} and v_0^{α} denote the slip direction and the slip plane normal to the slip system, respectively, in the initial unloaded configuration. The shearing rate on the each slip system depends on the resolved shear stress (τ_a) and the slip resistance (s_a) of that slip system.

3.2 Polycrystal model

Finite element calculations are conducted to make the transition from the response of a single grain (or a region within a grain) to the response of a polycrystalline aggregate. It is assumed that each element represents one crystal and is assigned an initial orientation [18, 21]. So each grain is modeled to allow for non-uniform deformation between the grains and within the grains, and both equilibrium and compatibility are satisfied in the weak finite element sense. In this study, we varied the number of elements, the number of grains in each element, and the distributions of grain orientations in mesh. In case of a multi-grain description the volume averaged stress is

$$\langle \boldsymbol{\sigma} \rangle = \sum_{k=1}^{N} \left(w_k \boldsymbol{\sigma}_k \right) \tag{4}$$

where $\langle \boldsymbol{\sigma} \rangle$ represents a volume average of Cauchy stress, N the number of total grains in the polycrystalline, w_k the volume fraction of each crystal, and $\boldsymbol{\sigma}_k$ the Cauchy stress in the k th crystal.

In metal forming process, the strain hardening of different materials will take place according to different rules. For FCC metal, strain hardening function $\dot{g}^{(\alpha)}$ can be expressed as

$$\dot{g}^{(\alpha)} = \sum_{\beta=1}^{n} h_{\alpha\beta} \left| \dot{\gamma}^{(\beta)} \right| \tag{5}$$

where $h_{\alpha\beta}$ is the hardening modulus matrix, $\dot{\gamma}^{(\beta)}$ is the shear strain rate led by the β th slip system. The parameter $h_{\alpha\beta}$ can be expressed as [18, 23-26]

$$h_{\alpha\beta} = q_{\alpha\beta} h^{\beta} = q_{\alpha\beta} h_0 \left\{ 1 - \frac{s^{\beta}}{s_s} \right\}^{l} \tag{6}$$

where h^{β} is the single slip hardening rate, and $q_{\alpha\beta}$ is a matrix describing the latent hardening behaviour of a crystallite. h_0, l and s_s are the hardening parameters of the slip system, s^{β} the slip resistance of the β th slip system. All the parameters for strain hardening of Al are shown in Table 2.

Table 2 Parameters for strain hardening of Al [18]

Parameter	Value
h_0	250 MPa
l	2.25
s_s	190 MPa
$q_{\alpha\beta}$	1.4

In plastic deformation, relationship between strain rate $\dot{\boldsymbol{\varepsilon}}$ and shear rates $\dot{\gamma}$ at the different slip systems can be shown as

$$\dot{\boldsymbol{\varepsilon}} = \sum_{\alpha=1}^{n} \frac{\dot{\gamma}^{\alpha}}{2} \left(s^{*(\alpha)} m^{*(\alpha)T} + m^{*(\alpha)} s^{*(\alpha)T} \right) \tag{7}$$

where, $s^{*(\alpha)T}$ is the transport matrix of the unit slip vector s^{*} of the α th slip direction in the initial configuration, $m^{*(\alpha)T}$ is the transport matrix of the unit normal vector m^{*} in slip plane of α th slip system in the initial configuration. In uniaxial planar compression. It can be expressed as

$$\dot{\boldsymbol{\varepsilon}} = \frac{\dot{\gamma}}{2\sqrt{6}} \begin{pmatrix} 16 & 0 & 0 \\ 0 & -8 & 0 \\ 0 & 0 & -8 \end{pmatrix} \tag{8}$$

3.3 Generation of 3D crystal plasticity finite element model

Three dimensional (3D) crystal plasticity finite element (CPFE) model is generated on a basis of AFM and EBSD experimental results. Actual crystal plasticity finite element model is generated as follows: from the AFM results, the main parameters of sample's surface asperity can be obtained, such as surface morphology, R_a and R_q. All these data will be input into Matlab, sorted and regenerated the surface morphology. All the data from Matlab will be employed to generate the surface of 3D CPFE model. We also used the results (grain size and grain orientations) from EBSD results to build up CPFE model by defining the properties of elements. The relationship between AFM measured results and Matlab calculated results and 3D CPFE model is shown in Fig. 4. Strain rate is an important parameter in the plastic deformation process (constitutive equations). We employed two kinds of strain rates in the CPFE model: one is $0.001s^{-1}$ (this one is for quasi-static process), the other is $0.01s^{-1}$. In this simulation, we employed different friction coefficient to model no lubrication and lubrication conditions. With lubrication, the employed friction coefficient is 0.02. Under condition of no lubrication, the applied friction coefficient is 0.2.

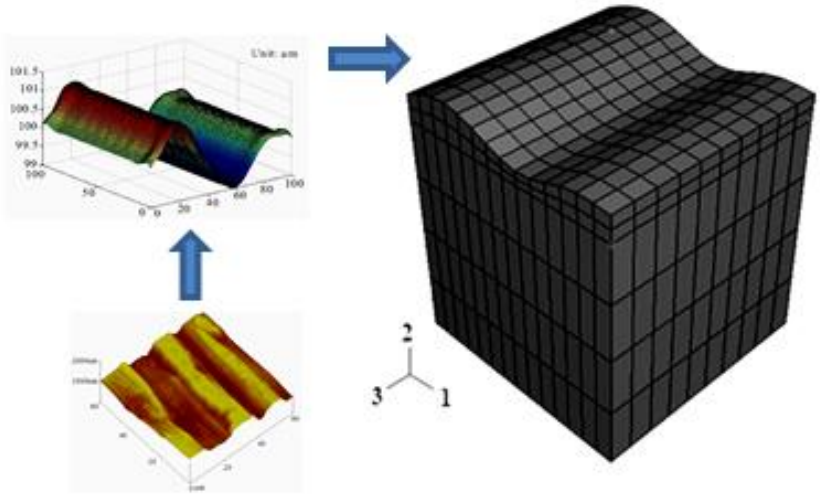

Figure 4 3D Generation of 3D crystal plasticity finite element model

4. Results and discussion

4.1 Development of surface asperity

From the previous research [18-21], it is obvious that the lubrication can play an obvious role in hindering the surface asperity flattening. If the surface asperity flattening takes place at quasi-static (very low strain rate) process, the influence of lubrication is similar. Fig. 5 shows the surface morphology of sample after the compression with 60% reduction. Lubrication plays

a significant role in the development of sample surface: it can hinder the surface asperity flattening process. In addition, if a sample is compressed with lubrication it will has a smooth surface with less surface scratch.

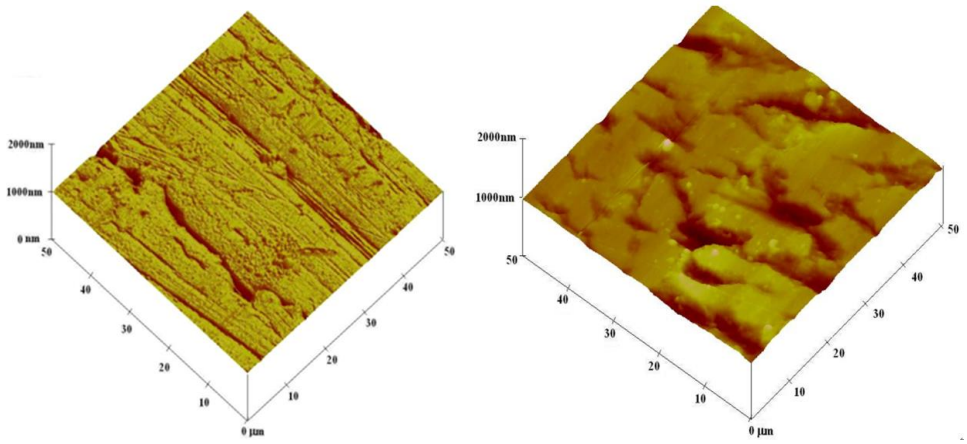

(a) (b)

Figure 5 Development of surface asperity under different condition of lubrication with a strain rate $0.001s^{-1}$: (a) without lubrication; (b) with lubrication.

4.2 Analysis of stress and strain

Fig. 6 shows the strain hardening process in cold quasi-static CUPC process. Stress is "force per unit area" - the ratio of applied force and cross section - defined as "force per area", which includes tensile stress, compressive stress and shear stress. Strain is defined as "deformation of a solid due to stress". It is obvious that compared to the sample compressed without lubrication, sample compressed with lubrication has a lower stress. In quasi-static process, with an increase of gauged reduction, the stress difference between the two samples is significant. The phenomenon is different from those compressed at a normal deformation rate. The reason for this is when sample compressed at a very low deformation rate, lubricant between the sample and tool will have enough time to fill the surface pits to fulfill its function.

On the other hand, the simulation results show a good agreement with the experimental results: it predicated the difference between the two samples, and the influence of lubrication on the stress. However, there is an obvious difference between the simulation result and experimental value. Though the predicated maximum stress for sample compressed with lubrication is similar to the experimental result, the maximum experimental stress for sample compress (about 380 MPa) without lubrication is much larger than that (about 300 MPa) from the simulation. The reason for the difference may be the friction coefficient between the sample

and tool which is employed in the model. The friction coefficient obtained from finite element (FE) modelling results is different from the employed one in Section 3.3: it is only 0.15 under the condition of no lubrication. While with lubrication, it is 0.0175. In current study, the used lubricant is molly bond, which is a solid lubricant. In further study, we maybe think about the existent of lubrication by fluid.

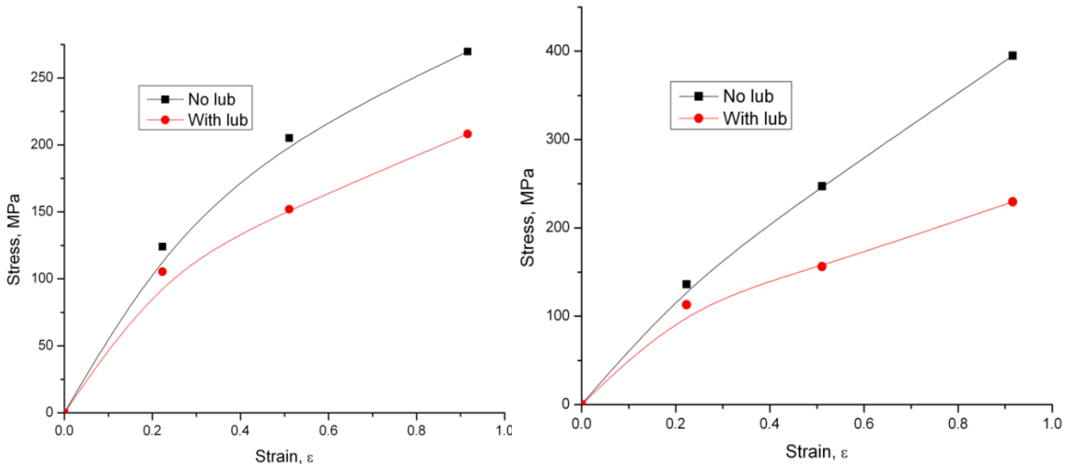

(a) (b)

Figure 6 Analysis of the relationship between stress and strain: (a) simulation results; (b) experimental results

4.3 Analysis of Pole figure

As mentioned above, the close packed plane in FCC metal is {111}. Therefore in this study, only pole figure {111} is employed to analyse the development of texture [25]. Before compression, the texture of sample is cubic texture {100} <001> (Fig. 7, reduction 0). If a sample is compressed with lubrication, surface textures in the edge area tends to develop from cubic orientation component {100} <001> to Goss orientation component {011} <100> in centre and a few symmetrical brass orientation component {011} <211> in the four edge areas (Fig. 7). However, if a sample is compressed without lubrication, copper orientation {112} <111> will generate along the horizontal symmetric axis and few anti-symmetric S orientation {123} <634> forms in edge area. Therefore, friction can promote the generation of copper orientation. Under the different lubrication conditions, surface local stresses are total different. Therefore, deformation textures in surface area are different. On the other hand, the simulated pole figures predicate the same tendency as the previous experimental results: with the increase of reduction, texture of sample tends to shift from annealed texture {100} <001> to the stabilised deformation texture {011} <211>. The simulated results also show the hindrance of

friction on texture development. However, the simulated results cannot predicate the S orientation {123} <634> obviously. In simulation, the constitutive model is simplified according to the five assumptions. Some shear stresses are not considered. Therefore the S orientation cannot be predicted.

Reduction	Modelling		Experiment	
	With lubrication	Without lubrication	With lubrication	Without lubrication
0 %	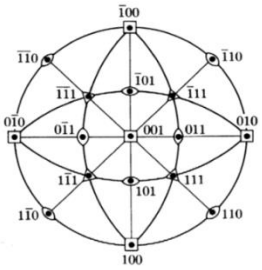	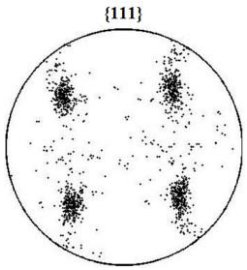	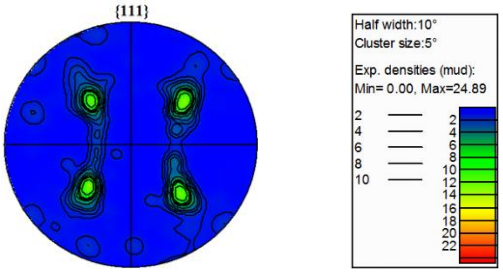	
20 %	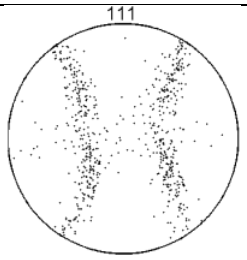	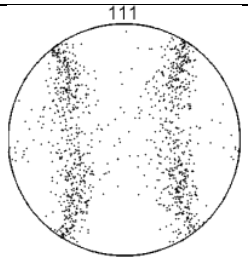	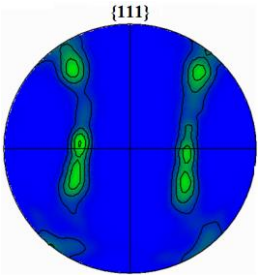	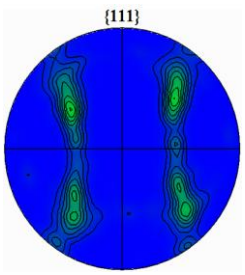
40 %	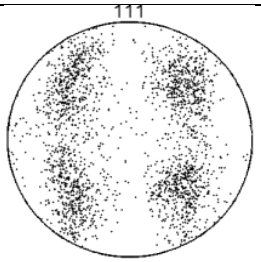	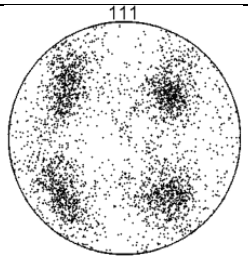	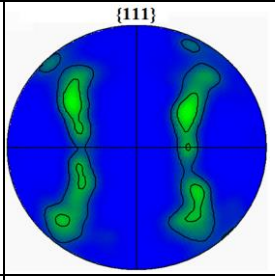	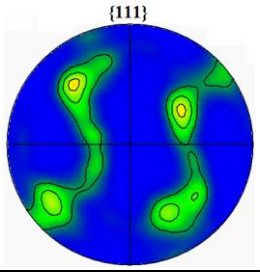
60 %	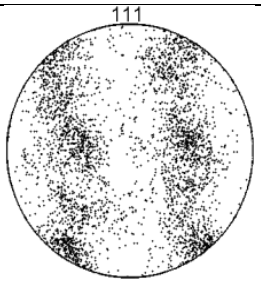	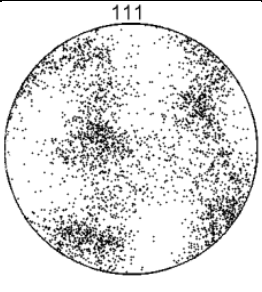	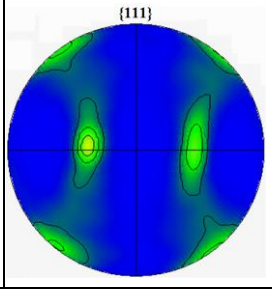	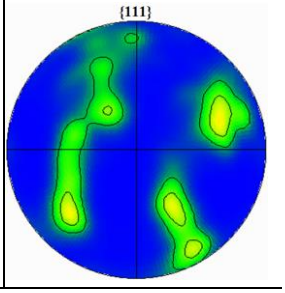

Figure 7 Analysis of Pole figure

4.4 Analysis of Taylor factor

Taylor factor is based on the Taylor plastic deformation theory, which assumed the active slip system combination will be the one which minimises the total sum of shears y_l on five dependent slip systems $\sum_l dy_l$ to accomplish the imposed strain $d\varepsilon$ [27, 28]. Therefore, the Taylor factor M can be defined as

$$M = \frac{\sum_l dy_l}{d\varepsilon} \tag{9}$$

where, *l* refers to the dependent slip system numbers, which ranges between 1 and 5.

Different from the Schmid factor, the Taylor factor shows the capability of plastic deformation resistance. It is not only a function of grain orientations, but also a function of external stress field. If the Taylor factor is high, it means the plastic deformation will be led by massive slip and consume large deformation work. While the Schmid factor only shows the stress that needed for the activation of the slip system and when the slip system can be activated.

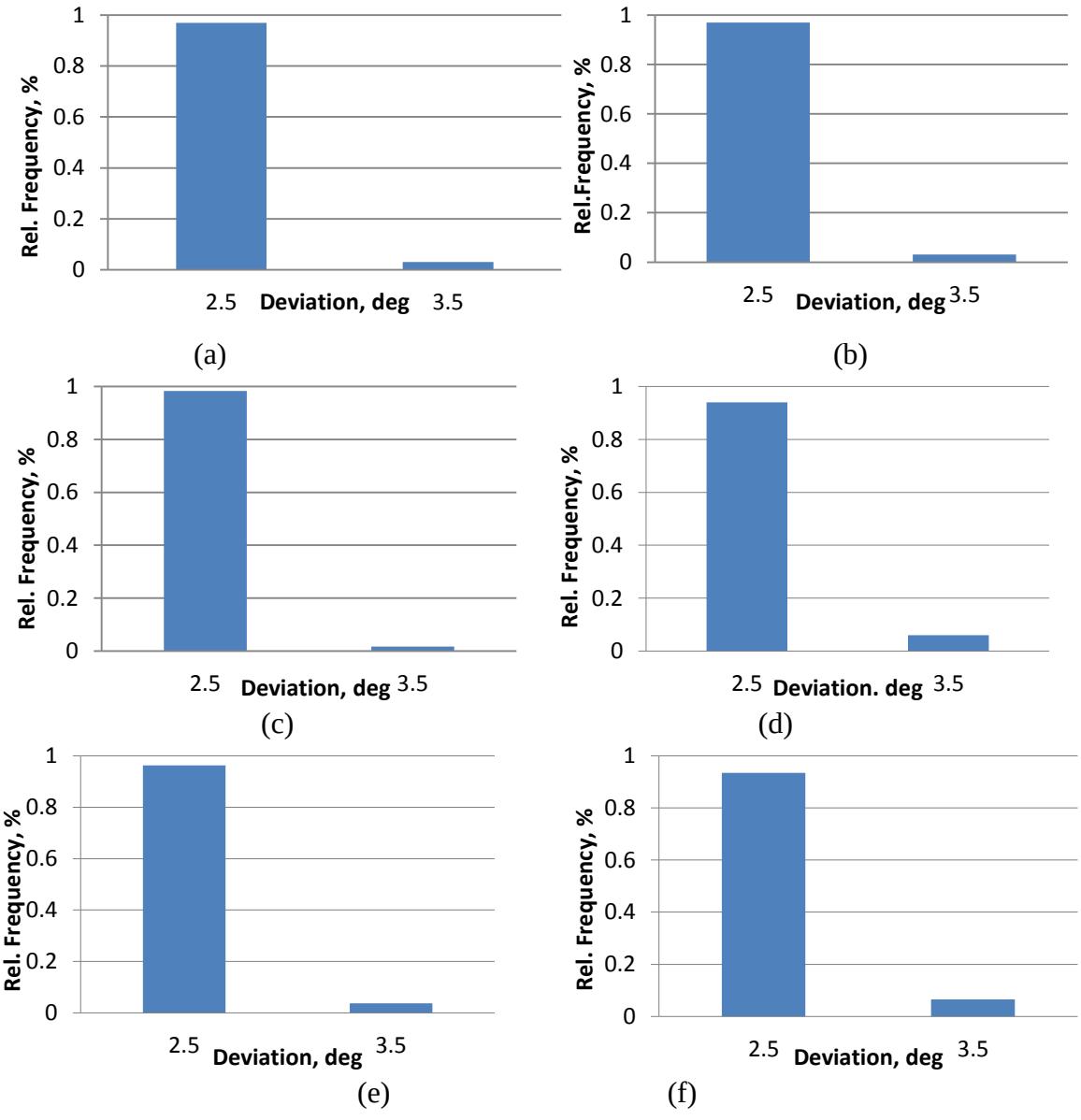

Figure 8 Analysis of Taylor factor under different conditions of lubrication: (a) 20% reduction, with lubrication; (b) 20% reduction, without lubrication; (c) 40% reduction, with lubrication; (d) 40% reduction, without lubrication; (e) 60% reduction, with lubrication; (f) 60% reduction, without lubrication.

In Figure 8, relative frequency refers to the number of times that different angle grain boundaries (GBS) occur. Deviation, deg refers to the angular deviation of different texture components. The value of deviation is chosen according to the sample material property. In cold quasi-static uniaxial planar compression, the gauged reduction plays an important role in the development of Taylor factor. With an increase of gauged reduction, the Taylor factor (in FCC, Taylor factor is about 3.06) tends to increase. This means the increased reduction can provide enough energy to activate more slip systems in this process. Lubrication can influence the Taylor factor obviously. Under the same gauged reduction, sample compressed with lubrication has the lower Taylor factor than the one compressed without lubrication (Fig. 8). That means compared to sample compressed with lubrication, the sample compressed without lubrication will have more slip systems to be activated, and in the process, the friction may become a drive to activate the slip system.

4.5 Analysis of coincidence site (CSL) boundary

CSL boundary is an abbreviation of coincidence site lattice boundary, which shows the coincidence points in two grain lattices after one grain lattice rotates along certain axis with certain angles [30]. A finite fraction of lattice sites coincide between the two lattices, then one can define a coincident site lattice (CSL). CSL boundary is a measure of grain boundary energy, impurity segregation behavior, migration rate of grain boundary. In this study, we used CSL to analyse the development of grain boundary energy in surface area during the surface asperity process. Normally Σ is used to express the CSL boundary, which is ratio of CSL and grain unit cell volumes [31]. In FCC metal Al, the typical grain boundary orientation includes $\Sigma=7$, $\Sigma=13a$, and $\Sigma=17$ [32]. So in this study, these three results are used for the analysis.

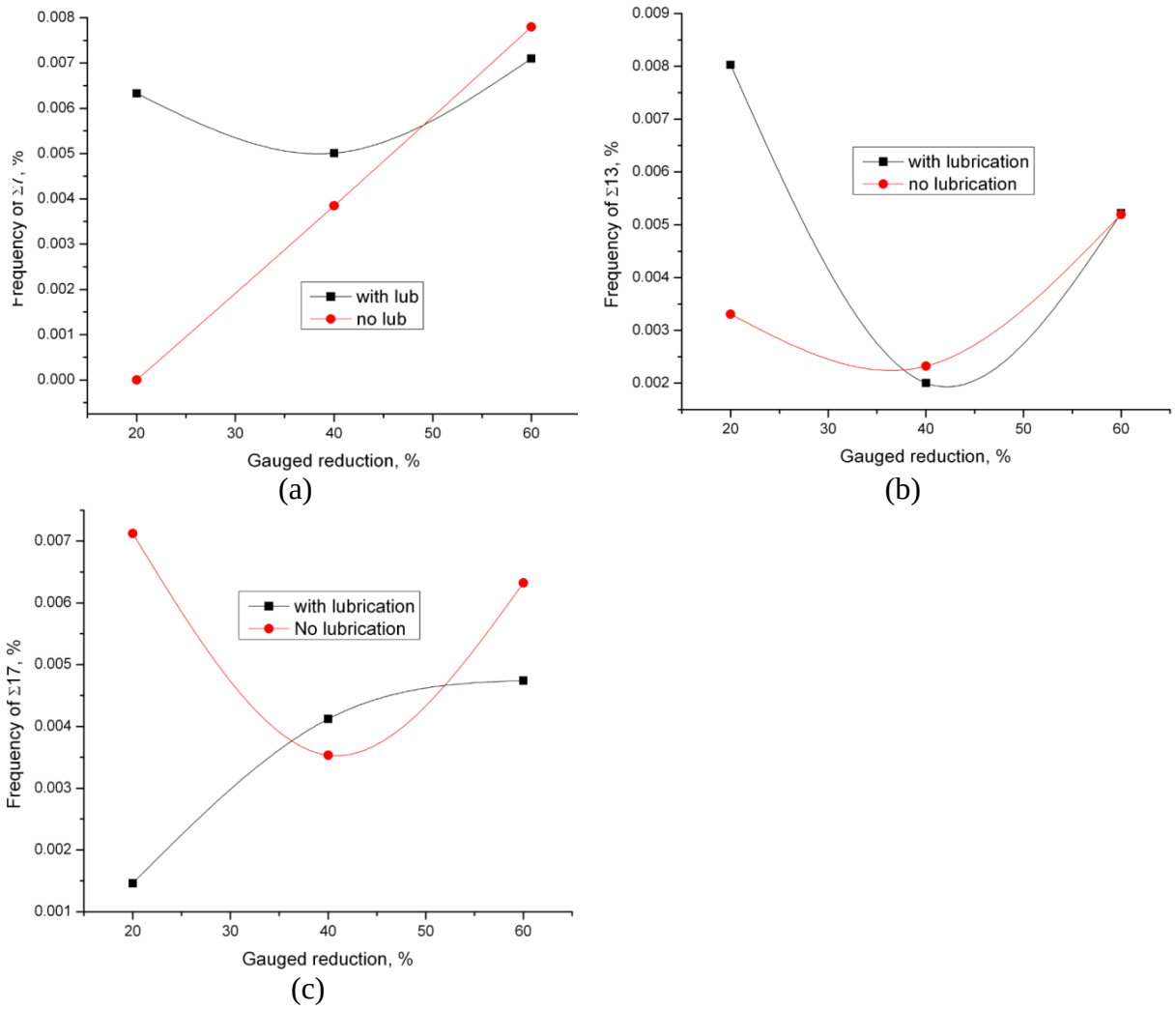

Figure 9 Development of typical CSL boundaries under different condition of lubrication: (a) Σ=7; (b) Σ=13a; (c) Σ=17

With an increase of gauged reduction, the Σ grain boundary shows the different tendencies. In Fig. 9 (a), the value of Σ7 grain boundary tends to increase greatly when the sample compressed without any lubrication, while the value of Σ7 grain boundary for the sample compressed with lubrication does not show an obvious increase. This means more grain lattices take place a rotation along the axis <111> with an angle of 40°. In the CUPC process, development of Σ7 grain boundary agrees with the tendency of surface asperity flattening. So we can guess that the migration of Σ7 may be the reason to the surface asperity flattening. Friction between the sample and compressing tool becomes the drive for the grain boundary migration. The other figure (Fig. 9 (b) Σ=13a) does not show any obvious tendency. In Fig. 9 (c), when the sample is compressed with lubrication, its value of Σ=17 grain boundary tends to increase significantly. This means with an increase of gauged reduction, more grain lattices in

the sample compressed with lubrication will take place a rotation along the axis <100> with an angle of 28.1°.

5. Conclusions

The conclusions can be drawn as:

(1) The simulation results show a good agreement with the experimental results. The crystal plasticity finite element model can effectively predict the surface asperity flattening process in this quasi-static deformation process, and show the role of lubrication in this process.

(2) Due to the limitation of the model and some parameters, the simulation results cannot predicate all the properties in details such as S orientation {123} <634>, the maximum stress is in sample compressed without lubrication.

(3) The experimental results also show, with an increase of gauged reduction, development of Taylor factor and CSL boundaries show the certain tendencies. Under the same gauged reduction, friction can increase the Taylor factor and Σ=7.

Acknowledgements:

The authors would like to thanks UOW Electron Microscopy Centre (EMC) for EBSD mapping and Mr. Cameron Neilson for the operation of CUPU process.

References

1. Liu, Z.L., You X.C., Zhuang. Z.: A mesoscale investigation of strain rate effect on dynamic deformation of single-crystal copper. Int. J. Solids. Struct. **45**, 3674–3687(2008)
2. Travis, L., Brown, A., Christopher, A., Tejas, G., Murthy, A.: A study of the interactive effects of strain, strain rate and temperature in severe plastic deformation of copper. Acta Mater. **57**, 5491–5500 (2009)
3. Serebrinsky, S.A., Duffo, G.S., Galvele, J.R.: Effect of strain rate on stress corrosion crack velocity difference between intergranular and transgranular cracking. Corros. Sci. **41**, 191-195 (1999)
4. Serebrinsky, S.A., Galvele, J.R.: Effect of the strain rate on stress corrosion crack velocities in face-centred cubic alloys. A mechanistic interpretation. Corros. Sci. **46,** 591–612(2004)
5. Wu, C.C., Wang, S.H., Chen, C.Y.: Inverse effect of strain rate on mechanical behavior and phase transformation of superaustenitic stainless steel. Scripta. Mater. **56**, 717–720 (2007)
6. Papakaliatakis, G.E.: Effect of strain rate on crack growth in aluminum alloy 1100-0. Theor. Appl. Fract Mec. **31**, 131-139 (1999)

7. Urcola, J.J., Sellars, C.M.: Effect of changing strain rate on stress-strain behaviour during high temperature deformation. Acta Mater. **35**, 2631-2647 (1987)
8. Takuda, H., Kikuchi, S., Tsukada, T. : Effect of strain rate on deformation behaviour of a Mg–8.5Li–1Zn alloy sheet at room temperature. Mater. Sci. Eng., A. **271**, 251–256 (1999)
9. Bhattacharyya, A., Rittel, D., Ravichandran, G.: Effect of strain rate on deformation texture in OFHC copper. Scripta Mater. **52**, 657–661 (2005)
10. Zhang, B., Shim, V.P.W.: Effect of strain rate on microstructure of polycrystalline oxygen-free high conductivity copper severely deformed at liquid nitrogen temperature. Acta Mater. 58, 6810–6827(2010)
11. Kodeeswaran, M., Gnanamoorthy, R.: Effect of strain rate on nanocrystalline surface formation in controlled ball impact process in AISI 304 SS. Mater Lett. **62**, 4516–4518 (2008)
12. Eghbali, B.: Effect of strain rate on the microstructural development through continuous dynamic recrystallization in a microalloyed steel. Mater. Sci. Eng., A. **527**, 3402–3406 (2010)
13. Percy, J. H.: The Effect of Strain Rate on the Forming Limit Diagram for Sheet Metal. Annals of the ClRP. **29**, 151-152 (1980)
14. Qin, K., Yang, L.M., Hu, S.S.: Mechanism of strain rate effect based on dislocation theory. Chin. Phys. Lett. **26**, 036103 1-4 (2009)
15. Li, H.J., Jiang, Z.Y., Wei, D.B., Han, J.T., Tieu, A.K.: Study on surface asperity flattening during uniaxial planar compression. Wear. **271**, 1778–1784 (2011)
16. Li, H.J., Jiang, Z.Y., Wei, D.B., Yan, P.J., Tieu, A.K., Han, J.T.: Crystal plasticity finite element modeling of surface asperity flattening during uniaxial planar compression. International Conference on Tribology in Manufacturing Processes. 397–406 (2010)
17. Li, H.J., Jiang, Z.Y., Wei, D.B.: Crystal plasticity finite modelling of 3D surface asperity flattening in uniaxial planar compression. Tribol. Lett. **46**, 101–112 (2012)
18. Li, H.J.: A study of surface roughness in the metal forming process, Ph.D Thesis, UOW, 2012.
19. Li, H.J., Jiang, Z.Y., Wei, D.B.: Wear. **301**, 11–18 (2013)
20. Li, H.J., Jiang, Z.Y., Wei, D.B.: Tribol. Int. **66**, 282–288 (2013)
21. Li, H.J.,, Jiang, Z.Y., Wei, D.B.: Tribol. Lett. **46**, 101–112 (2013)
22. Asaro, R.J., Needleman, A.: Texture development and strain hardening in rate dependent polycrystals. Acta Metall. **33**, 923–953 (1985)
23. Kalidindi, S.R., Schoenfeld, S.E.: On the prediction of yield surfaces by the crystal plasticity models for FCC polycrystals. Mater. Sci. Eng., A. **293**,120–129 (2000)
24. Kalidindi, S.R., Anand, L.: Macroscopic shape change and evolution of crystallographic texture in pre-textured FCC metals. J. Mech. Phys. Solids. **42**, 459–490 (1994)
25. Kalidindi, S.R., Anand, L.: An approximate procedure for predicting the evolution of crystallographic texture in bulk deformation processing of FCC metals. Int J. Mech. Sci. **34**, 310–312 (1992)
26. Kalidindi, S.R., Bronkhorst, C.A., Anand, L.: Crystallographic texture evolution in bulk deformation processing of FCC metals. J. Mech. Phys. Solids. **40**, 552–555 (1992)
27. Taylor, G.I.: Plastic strain in metals. J. Inst. Met. 62-307-324(1938)
28. Rosenberg, J. M., Piehler, H. R.: Calculation of the taylor factor and lattice rotations for bcc metals deforming by pencil glide. Metall. Mater. Trans. B. **2**, 257-259 (1971).

29. Justinger, H., Hirt, G.: Estimation of grain size and grain orientation influence in micro-forming processes by Taylor factor considerations. J. Mater. Process. Tech. **209**, 2111–2121(2009).
30. Mao, W.M., Yang, P., Cheng. L.: Analysing principles and test techniques of material texture. Metallurgical industry press, 2008.
31. WARRINGTON, D. H.: The coincidence site lattice (CSL) and grain boundary (DSC) dislocations for the hexagonal lattice, J. Phys. Colloques. 36, C4-87-C4-95 (1975)
32. Yang, P.: EBSD technique and application. Metallurgical industry press, 2007.